Journal of Nanobiotechnology

RESEARCH Open Access

A green, versatile, and facile strategy for anti-biofouling surface with ultra-high graft density polyethylene glycol

Wenjie Liu[1,2], Suqin He[1*], Hao Liu[1], Zeyu Shou[2,3], Kaiyuan Huo[2], Hongping Xiang[4], Aihan Feng[4], Wei Lu[5*] and Na Li[2*]

Abstract

Implantable catheters are susceptible to severe complications due to non-specific protein adhesion on their surfaces. Polyethylene glycol (PEG) coatings, the gold standard for resistance to non-specific protein adhesion, present a challenge in achieving high-density grafting, which significantly restricts their use as anti-biofouling coatings. Herein, we exploited the strong interaction between polyphenols (PCs) and polycations (K6-PEG) to graft PEG onto the surface of PC-Cu (A network of metal polyphenols composed of proanthocyanidins and metal copper ions, with expectation for the coating with excellent resistance to non-specific protein adhesion (PC-Cu@K6-PEG). The introduction of K6-PEG resulted in enhanced stability and modulus of PC-Cu, as well as a reduction in the surface adhesion energy and contact angle of PC-Cu. In contrast to previously reported PEG coatings, PC-Cu@K6-PEG exhibited a markedly elevated grafting density of PEG (4.06 chains/nm^2), which was more than double the highest value previously reported (1.9 chains/nm^2), due to the diffusing ability of K6-PEG throughout the PC-Cu networks. PC-Cu@K6-PEG displays robust resistance to a variety of proteins, microbials, and platelet attachment, thereby preventing thrombosis. The coating ability of PC-Cu onto diverse substrates, combined with the simple, straightforward and environmentally benign process of fabricating PC-Cu@K6-PEG, suggests that this strategy has significant potential for use in anti-biofouling surfaces.

Keywords Non-specific adsorption, Anti-biofouling coating, Peptide, Polyethylene glycol (PEG), Metal-phenol networks (MPNs)

Introduction

In the medical field, the need for antifouling coatings is increasing as many devices require direct contact with human tissue, such as implants, catheters, sensors, due to the anti-biofouling coatings not only enhancing the protective performance of medical devices, but also significantly improving the clinical experience and safety and security of patients by improving biocompatibility [1]. For example, catheters as one of the most important medical product categories and currently used for a wide range of medical conditions, the incidence of bacterial infections and thrombosis is as high as 5–15% and 10–20%, respectively [2–4]. These can lead to serious catheter-related

*Correspondence:
Suqin He
hesq@zzu.edu.cn
Wei Lu
luwei@wmu.edu.cn
Na Li
lina0701@ucas.ac.cn

Full list of author information is available at the end of the article

Graphical abstract

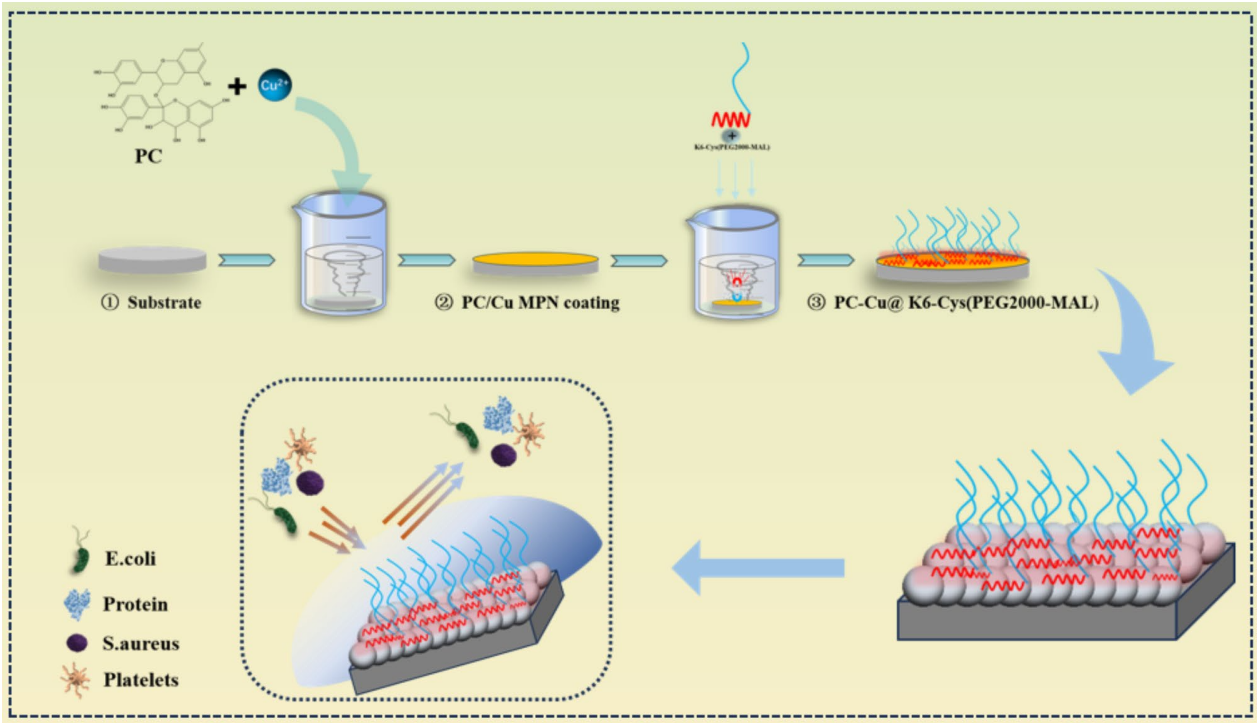

consequences, such as sepsis and deep vein thrombosis [5]. The main cause is attributed to non-specific adhesion of proteins. Non-specific adhesion of proteins induces bacteria easily adhere to the surface of catheter materials, secreting extracellular matrix and multiply, and further forming a difficult-to-remove bacterial biofilm, leading to a variety of infections and inflammatory responses [6, 7]. When exposed to the bloodstream, non-specific protein adhesion results in platelet adhesion and activation, fibrin formation, and eventual thrombus formation through interaction with fibrinogen and thrombin, causing death of patient in some serious cases [8]. Over the past decades, the mainstay of systemic therapy has long relied on the systemic use of anticoagulants and antibiotics. However, overdosing of these drugs may be plagued by several problems, such as heparin-induced postoperative bleeding and hyperkalemia, and bacterial resistance caused by long-term antibiotic use [9]. The development of implantable devices with a high level of resistance to protein adsorption (anti-biofouling) is therefore of great importance for public health.

Engineering the surface of catheters that resist non-specific protein adsorption is considered an effective means. Various coating materials, such as polyethylene glycol (PEG), poly-2-oxazoline, poly(hydroxyethylmethacrylate) and poly[N-(2-hydroxypropyl) methacrylamide] have been coated on different substrate materials and shown to reduce the adsorption of non-specific proteins [10]. Among these, polyethylene glycol (PEG) is considered to be a most effective coating material due to its strong resistance to hydration and spatial location and has been widely used in the manufacture of anti-biofouling surface materials [11, 12]. There are generally two main categories, graft from (GF) and graft to (GT) [13, 14], in the preparation of anti-biofouling coatings. The GF method is a surface initiated (SI) polymerisation process, in which the polymer chains are grown in situ from initiator molecules attached onto the surface. The generation of polymer brushes on the material surface is usually achieved by controlled radical polymerisation such as atom transfer radical polymerisation (ATRP) and reversible addition chain transfer polymerisation (RAFT) [15]. For example, Nagasaki [16–18]et al. designed a series of PEGs capped with different groups (which contained N6 (pentaethylenehexamine), PAMA (poly[2-(N, N-dimethylamino) ethylmethacrylate]); -SH (thiols), etc.) to bind to gold surfaces via the groups capped at the end of the PEG chain, resulting in a nonspecific antiprotein adsorption effect on the gold surface sensor. Later, mussel-inspired bioadhesion techniques were widely used to adapt to different material surfaces. For example, Meagher [19] et al. generated poly(ethylene glycol methyl ether methacrylate) (MW~475) (PEGMA) polymers in situ on various substrates by surface-initiated ATRP (SI-ATRP) and showed

good resistance to static fouling. In the GT process, pre-synthesised polymer chains from a melt or polymer solution are attached to either physically or chemically a surface through a process known as 'tethering'. For instance, Messersmith et al. [20, 21] employed 3,4-dihydroxyphenylalanine (DOPA), derived from mussel adhesion protein (MAP), to affix polyethylene glycol (PEG) to a titanium dioxide (TiO_2) substrate, thereby imparting the material with resistance to protein adsorption.

Previous studies have shown that the length and grafting density of the PEG chains on the surface have a close relationship with the resistance to protein adsorption. Among these, the graft density has been the focus of research because a high graft density can form a denser hydration layer and fill in the voids or the defects on the surface that the brushes do not cover. GT is simple and straightforward, but limiting the density of grafted PEGs by preventing further attachment when existing PEGs begin to adhere to the surface [22]. In contrast, GF is a bottom-up approach, which in principle makes it easier to achieve high-density grafted brush layers. However, due to the self-termination effect of the free radical reaction and the reduced reactive grafting activity caused by the spatial resistance of the PEG molecular brushes, the preparation of high-density grafted brush by GF is still a big challenge. The reported maximum grafting density of PEG was 0.79 chains/nm² and 1.9 chains/nm² for the GF and GT strategy, respectively [12, 23]. Besides, the GF method requires the maintenance of radical activity over a long period of time and harsh reaction conditions, which makes its industrial application challenging [24]. Both for GT and GF methods, the use of organic reagents is usually involved, which leads to concerns about biosafety. In addition, introducing anti-biofouling coatings to implant surfaces in a rational and effective manner is a major challenge due to the diversity of catheter materials. Therefore, a general, simple and effective green strategy for high-density surface polymer brush grafting is urgently needed.

Metal-polyphenol networks (MPNs) formed by the coordinative interaction between metal ions and phenolic ligands in polyphenol MPNs have received increasing attention due to their fast and simple deposition process on different shapes and a wide range of substrates (silicon, quartz, gold and polypropylene sheets, etc.), since the report by Caruso et al. [25]. It has been shown that MPNs have a certain degree of inherent anti-biofouling ability, attributed to a certain degree of hydrophilicity on their surfaces [26]. However, polyphenols are prone to non-specific adsorption of proteins and polysaccharides through multiple interactions, which can lead to unexpected biological events. In addition, the long-term stability of polyphenols is difficult to ensure due to their susceptibility to oxidation, which also limits the potential of MPNs for anti-biofouling applications.

There are strong and diverse interactions between polyphenols and polycations, including hydrogen bonding, hydrophobicity and electrostatic interactions, which can be used to separate polyphenols and create functional coatings. For example, Xu, F. et al. [27] describe the co-substitution of tannic acid with alkyl and quaternary ammonium groups to construct a cationic coating material (AQTA), which was then used to functionalise a multifunctional medical device for antimicrobial and haemostatic applications. In our group's previous studies, functional peptides were introduced into polyphenol-based coatings via positively charged K6 (hexameric lysine) in order to achieve enhanced osseointegration of implants [28, 29]. Herein, by linking PEG to short positively charged peptide, hexameric lysine (K6), we fabricated an anti-biofouling coating on pre-constructed PC-Cu MPNs coating onto diverse substrates through a green process (Fig. 1a). Our results demonstrated that the introduction of polyethylene glycol (PEG) was not a classical adsorption process that occurs only on the surface, but a process of penetration into the whole PC-Cu MPNs coating, which leads to PEG layer with a markedly elevated grafting density (4.06 chains/nm²) and long-lasting anti-biofouling properties and resistance to the attachment of proteins, microorganisms and platelet, and avoidance of thrombosis (Fig. 1b).

Experimental section

Chemicals and materials

Proanthocyanidins (PC, 95%), anhydrous copper chloride ($CuCl_2$, 98%), and tris(hydroxymethyl)aminomethane (Tris) (≥99%), sodium chloride (NaCl, 99.99%), Urea (99.99%), Tween 20, Sodium hydroxide (NaOH) (AR), ammonia (AR), dexamethasone and sodium β-glycerophosphate (β-GP, 13408-09-8) were purchased from Macklin. K6-PEG was ordered from Hangzhou Specific Peptide Biologicals Ltd. with purity > 95%, MW = 3095.37). All chemicals were used without any purification. FITC-labeled bovine serum proteins and lysozyme were synthesized by coupling FITC to the free ϵ-amino group of the proteins to form a thiourea bond, according to reported method [30]. Hemoglobin was purchased from Te Ai (Shanghai) Chemical Industry Development Co. Ltd, Mucins and Fibronectin were purchased from Shanghai Yuan Ye Biotechnology Co. Ltd, Escherichia coli (DH5α) and Staphylococcus aureus (SH1000). LIVE/DEAD BacLight Bacterial Viability Kit was purchased from ThermoFisher Co. Silicon wafers, titanium (Ti) plates, and circular glass coverslips (14 mm diameter, nested) were cleaned with piranha solution (70% H_2SO_4 and 30% H_2O_2, V/V) for 2 h at 98 ℃, then rinsed with MILI-Q water and dried in a gentle air stream before use

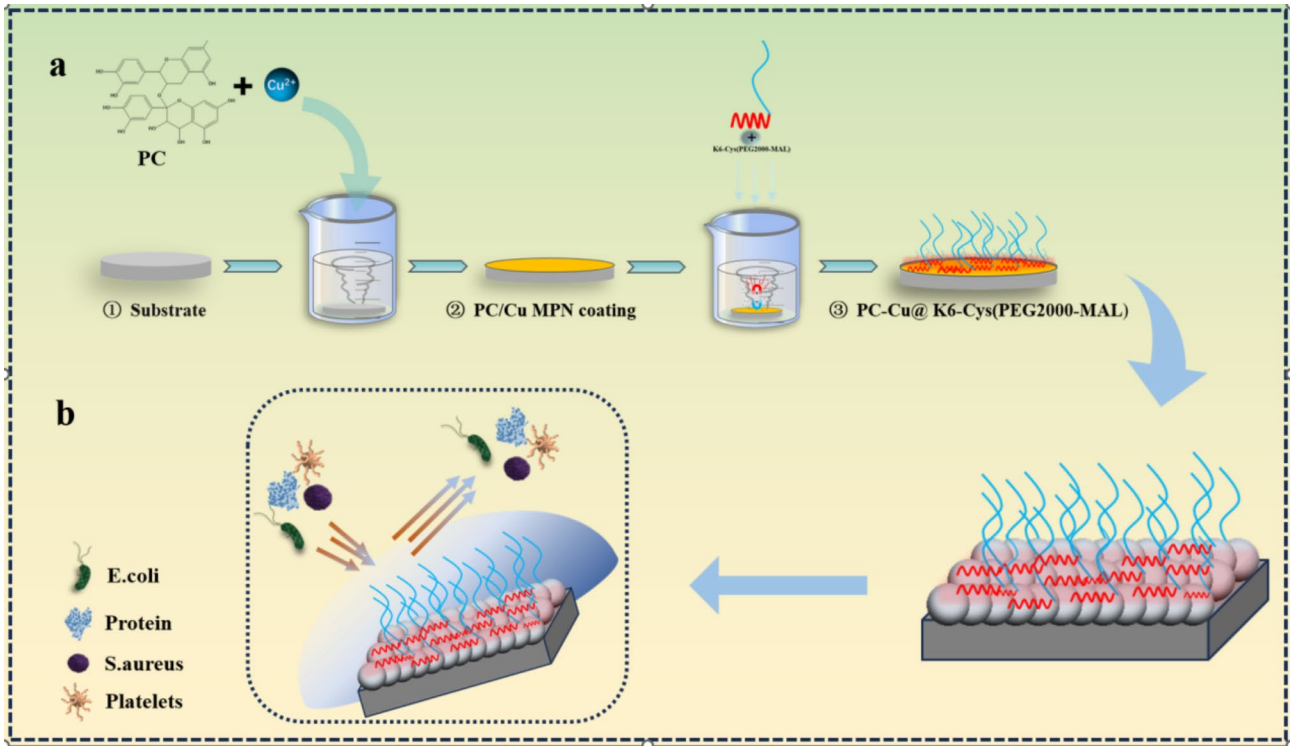

Fig. 1 (**a**) Preparation process of the PC-Cu@K6-PEG coating; (**b**) Schematic representation of the PC-Cu@K6-PEG coating anti-biofouling (proteins; bacteria; platelets)

(Note: piranha solution is highly oxidizing and corrosive and should be prepared and used with extreme caution). Experiments with deionized (DI) water purified using the MILI-Q system have a resistivity in excess of 18.25 MΩ·cm.

Preparation of PC-Cu@K6-PEG coating

The components were assembled on clean, treated wafers (including PC-Cu MPNs substrates and K6-PEG surface layers). The silicon substrate was immersed in 500 µl of PC solution (concentration of 3 mM, dissolved in deionised water, pH 5.5). The pH was then adjusted to 5.5 with 0.1 M sodium hydroxide. Finally, 500 µl of Subsequently, a solution of $CuCl_2$ (concentration of 5 mM, dissolved in deionised water, without adjusting the pH) was added, and the silicon wafer was then shaken on the shaking table (at 800 rpm) for 30 s. Following this, the wafer was left to stand for 10 min. Following 30 s shaking period (at 200 rpm) and a 10-minute resting period, 500 µl of Tris-HCl buffer (100 mM, pH 8) was added and mixed for 30 s. The silicon wafer was then removed and the surface was rinsed slowly with deionised water, and then blown dry with nitrogen to obtain a layer of MPN. The aforementioned steps were repeated in order to obtain MPNs with varying numbers of layers per cycle, which were recorded as MPNn (n=5, 10, 20)(The following defaults to n=10 unless explicitly stated). For subsequent grafting of K6-PEG, the aforementioned procedure is typically repeated at least five times. Prior to commencing the subsequent step, the coatings were immersed in PC solution, removed and rinsed, and then immersed in K6-PEG (1 mg/mL) (dissolved in Tris-HCl (10 mM, pH 9)) and placed on a shaker (at 70 rpm) for 24 h. Subsequently, the coatings were removed and rinsed thoroughly with deionised water, and then blown dry with nitrogen gas to obtain the PC-Cu@K6-PEG coatings(All the above experimental procedures were carried out at room temperature). All the pH adjustments mentioned above were made using 1 mM salt. Specifically, 1 mM hydrochloric acid and 1 mM sodium hydroxide were used for the above pH adjustments. In order to meet the requirements of subsequent experiments, the coatings were also applied to glass substrates with a diameter of 14 mm and to gold substrates. The procedure was identical to that previously described.

Thickness test

The ellipsometric spectroscopy model (SE) can accurately monitor the changes in polarization state of incident light waves at material interfaces upon reflection by measuring the polarizing angle (ψ) and phase difference (Δ), and also can calculate the refractive index, thickness, and quality of the information interface coating. The Woollam M2000UI ellipsometric spectrometer (J.A. Woollam Co.,

Inc., Lincoln, NE) was utilized, with WVASE32 serving as the analysis software, employing two incident angles, 65 ° and 70 °. The values of ψ (polarization angle) and Δ (phase) were measured between 245 and 1000 nm. These two parameters (ψ and Δ) are related to the thickness and optical properties of the sample and can be calculated using the following equations:

$$\mathbf{tan}\psi\mathbf{e}^{\mathbf{i}\Delta} \equiv \frac{\mathbf{r_p}}{\mathbf{r_s}} \equiv \rho\left(\theta_0, \mathbf{h}_1, \ldots, \mathbf{h_j}, \mathbf{N_a}, \mathbf{N_S}, \mathbf{N}_1, \ldots, \mathbf{N_j}\right)$$

where r_p and r_s are the reflection coefficients parallel and perpendicular to the incident surface, respectively, ρ is the complex reflectance, θ_0 is the angle of incidence, h_j is the thickness of the layer, and N_a, N_s, and N_j are the complex refractive indices of the environment, substrate, and layer, respectively.

X-ray photoelectron spectrometer

The assembled PC-Cu coatings and PC-Cu@K6-PEG coatings were characterized using X-ray photoelectron spectroscopy (ESCALAB 250) to obtain peak data under the conditions of a take-off angle of 90 ° and an energy of 20 eV. In this case, the PC-Cu@K6-PEG layer was etched twice, each time with a thickness of 15 nm and a cumulative etch depth of 30 nm.

Water contact angle (WCA) characterization

The contact angle is the angle between the solid-liquid interface passing through the liquid interior and the gas-liquid interface. In research, the WCA is commonly used to measure the hydrophilicity of materials. This experiment used the static contact angle drop method using the KRUSS DSA1 1.80 version contact angle analyzer. Deionized water was used as the probing droplet to measure the WCA of the samples. Specifically, 5 μL of ultrapure water was precisely dropped onto the sample surface, and the moment of contact between the ultrapure water and the sample surface was captured using a high-speed camera. Then use OneAttension software to analyze the size of the WCA.

Mechanical performance testing

Surface mechanical properties, adhesion, and roughness of the coatings were measured using an atomic force microscope (AFM, Dimension Icon, Bruker). Firstly, the samples were placed on the AFM sample stage and securely fixed using vacuum adsorption. Subsequently, the surface of the coating samples was characterized using the tapping mode of MikroMash silicon cantilevers, and roughness was calculated using accompanying software. To calculate the Young's modulus, the Derjaguin-Muller-Toporov model was employed to fit the retraction curves of force versus separation obtained from the AFM measurements. The principle of adhesion energy testing involves applying appropriate force to the coating using an AFM probe. As the probe approaches the coating, it experiences attractive forces. Upon contact with the coating, these attractive forces transform into repulsive forces, and the measured force corresponds to the adhesion energy of the coating.

Stability and hydrophilic of PC-Cu@K6-PEG coatings

The stability of the hydrophilicity of the PC-Cu@K6-PEG coatings was evaluated by immersing the PC-Cu@K6-PEG coatings in PBS (pH 7.3) for 0–7 days or irradiating them continuously with UV for 24 h, and then measuring the WCA on the surface of the blown-dry samples by the static solid-drop method. The ability of the samples to withstand extreme environments was evaluated by immersing the PC-Cu MPNs coatings with the PC-Cu@K6-PEG coatings in pH=2 and pH=12 solutions, and measuring the thickness of the immersed thicknesses by optical ellipsometry (M-2000UI, J.A. Woollam).

Calculation of surface graft density of PC-Cu@K6-PEG coatings

The grafting density (δ) of K6-PEG on the PC-Cu surface was calculated using the following equation:

$$\delta = \frac{\rho \mathrm{S} \Delta \mathrm{L} \mathrm{N_A}}{\mathrm{MS}}$$

In this context, the symbol S denotes the grafted area. It is assumed that the density of K6-PEG, denoted by the symbol ρ, is 1 g/cm³. The symbol ΔL denotes the thickness of the K6-PEG contribution. The symbol N_A denotes Avogadro's constant. The symbol M denotes the molecular weight of K6-PEG. Finally, the symbol δ denotes the grafting density.

Quartz crystal microbalance (QCM-D)

The antisorption process of the coating on the surface of the gold base against proteins was monitored using a quartz crystal microbalance (QCM-D) with a dissipation function. The gold-plated quartz crystal sensors were subjected to a cleaning process involving a solution of ammonia (25%), hydrogen peroxide (30%), and water (1:1:5) at a temperature of 75 °C for one hour. This was followed by a comprehensive rinsing with deionized water and drying under nitrogen. Subsequently, the gold-plated quartz crystal sensor was mounted in the flow chamber of the Q-Sense instrument and a phosphate-buffered saline (PBS) buffer solution was flowed through the chip until the system reached equilibrium. Subsequently, a variety of proteins (dissolved in PBS, pH=7) were introduced into the system in a sequential manner, resulting in a discernible shift in the resonant frequency

before reaching equilibrium once more. Finally, the PBS solution was circulated through the chip to remove any residual proteins that had not adhered to the surface. The injection solution was injected at a flow rate of 100 μL/min, and the change in resonance frequency (Δf) was monitored in real time at different harmonics (ν=3, 5, 7, 9, etc.). The ν=3 data were used for image plotting.

Protein adsorption test

The ability to non-specifically passivate the adsorption of a wide range of proteins is key to achieving biofouling. We measured the magnetic changes of different proteins (bovine serum proteins, lysozyme, fibrinogen, mucin, and hemoglobin) during the flow over the surface of the chips coated with PC-Cu MPNs and PC-Cu@K6-PEG coatings, respectively using a quartz crystal microbalance with dissipation (QCM-D). In addition, the amounts of proteins adsorbed on the surface of the gold sensor was further obtained by Sauerbrey formula fitting. In order to visualize the effect, we incubated FITC-labeled bovine serum proteins as well as lysozyme with the materials at 37 °C for 24 h. After removal, we blocked the slices under light-avoidance conditions, captured the images with a laser confocal microscope, and semi-quantitatively analyzed the fluorescence using the software image J.

Bacterial adhesion test

Antimicrobial adhesion activity of the surfaces was tested using Gram-positive (Staphylococcus aureus) and Gram-negative (Escherichia coli) bacteria; firstly, *E. coli* and *S. aureus* epidermidis were incubated for 24 h on agar solids at 37 ℃, and then passaged twice to ensure monoclonality. Subsequently, a set of fresh colonies was selected and dispersed in LB medium and shaken overnight in a 37 ℃ incubator. The next day, 100 μl of the bacterial solution was aspirated in a 96 wells plate for counting, and then the bacteria were resuspended in a solution containing 0.2% liquid medium and 99.8% physiological saline (maintaining a bacterial concentration of 10^7 cfu/ml). Apply 500 μl of bacterial solution to the sample surface. After incubation at 37 ℃ for 8 h, the surface bacteria were slightly rinsed with saline and then fixed with 2.5% glutaraldehyde solution overnight. After further dehydration, the bacterial attachment to the sample surface was observed by scanning electron microscopy (SEM). Furthermore, following the 24 h incubation of the bacteria on the sample surface, the bacteria were removed by washing with saline. A bacterial live-dead dye was then added to the samples, which were incubated at 37 °C for 20 min. The samples were subsequently blocked in a closed environment and observed under a laser confocal microscope. The bacterial adherence on the coated surfaces was analysed fluorescently and semi-quantitatively using the software Image J.

Hemolysis

Fresh whole blood from rabbits (purchased from Zhejiang Laboratory Animal Centre) was centrifuged at 4 °C for 15 min (1500 rpm) to obtain an erythrocyte suspension. The suspension was then washed with saline and centrifuged at 1500 rpm for 3 min. This process was repeated at least three times until the supernatant was clear. The collected erythrocyte suspension was then diluted to 4% by volume with saline. Place the sample in a 1.5 ml test tube. The diluted suspension (500 μL) and saline (500 μL) were added to each well and incubated with the samples at 37 °C for 1 h. Meanwhile, the cell suspensions of the negative and positive control groups were incubated with saline and 0.2% Triton solution without sample, respectively. The cell suspension was then centrifuged at 2000 rpm for 3 min to obtain the supernatant. Finally, 150 μL of supernatant from each group was transferred to a 96 wells plate and OD 540 was read using an enzyme-linked immunosorbent assay (Biotek, USA):

$$Hemolysis\ ratio\,(\%) = \frac{\text{OD samples} - \text{OD negative}}{\text{OD positive} - \text{OD negative}}$$

Platelet adhesion test

Samples were placed in 12 wells plates and equilibrated with PBS overnight. All samples were then immersed in 2 mL of PRP (obtained by centrifuging fresh blood at 1500 rpm/min for 15 min) and incubated at 37 °C for 3 h. After incubation, samples were washed with PBS to remove nonadherent platelets and then fixed with 2.5% glutaraldehyde solution at 4 °C for 4 h. The samples were subjected to a series of grades of ethanol (25%, 50%, 75%, 95%, and 100%, v/v) at room temperature for 30 min per step and dried under vacuum. The morphology and number of platelets adhering to the surface of the samples were observed using field emission scanning electron microscopy.

Ex vivo thrombogenicity

Nine New Zealand White rabbits (purchased from the Zhejiang Animal Experiment Centre) were randomly divided into three groups (3 rabbits in each group) were anaesthetised with sodium pentobarbital at a concentration of 30 mg/ml and a dose of 1 ml/kg. The left carotid artery and right external jugular vein were surgically exposed and cannulated. PU catheters (unmodified, PC-Cu MPNs-modified and PC-Cu@K6-PEG-modified) were then attached at one end to the rabbit jugular vein and at the other end to the rabbit carotid artery to create a closed circulatory system. After 2 h of in vitro circulation, the unmodified, PC-Cu MPNs-modified and PC-Cu@K6-PEG-modified PU tubes were removed and rinsed three times with saline. The thrombus weight of

the tubes was determined by weighing the tubes before and after the experiment, and the catheter occlusion rate was quantified by calculating the percentage of lumen area occlusion using computerized image analysis. The rabbits were anaesthetized using gas and subsequently euthanized by cervical dislocation.

Statistics analysis

Statistical significance was tested by ANOVA, with $p<0.05$ considered significant: $^{*}p<0.05$, $^{**}p<0.01$, $^{***}p<0.001$. Error bars represent the standard deviation of the mean for each type of experiment, which was repeated at least three times for each experimental group.

Ethics approval and consent to participate

The protocol for all animal implantation surgeries was approved by the Wenzhou Institute, University of Chinese Academy of Sciences, with ethics number WIUCAS24022602. All procedures were conducted by following the standards described in the guidelines for the care and use of laboratory animals. All procedures were conducted by following the standards described in the guidelines for the care and use of laboratory animals.

Results and discussion

Characterization of coatings

The PC-Cu MPNs coatings were prepared by self-assembly in the aqueous phase, as previously reported [31]. Subsequently, K6-PEG was deposited onto the MPNs coatings by immersing MPNs into K6-PEG solution

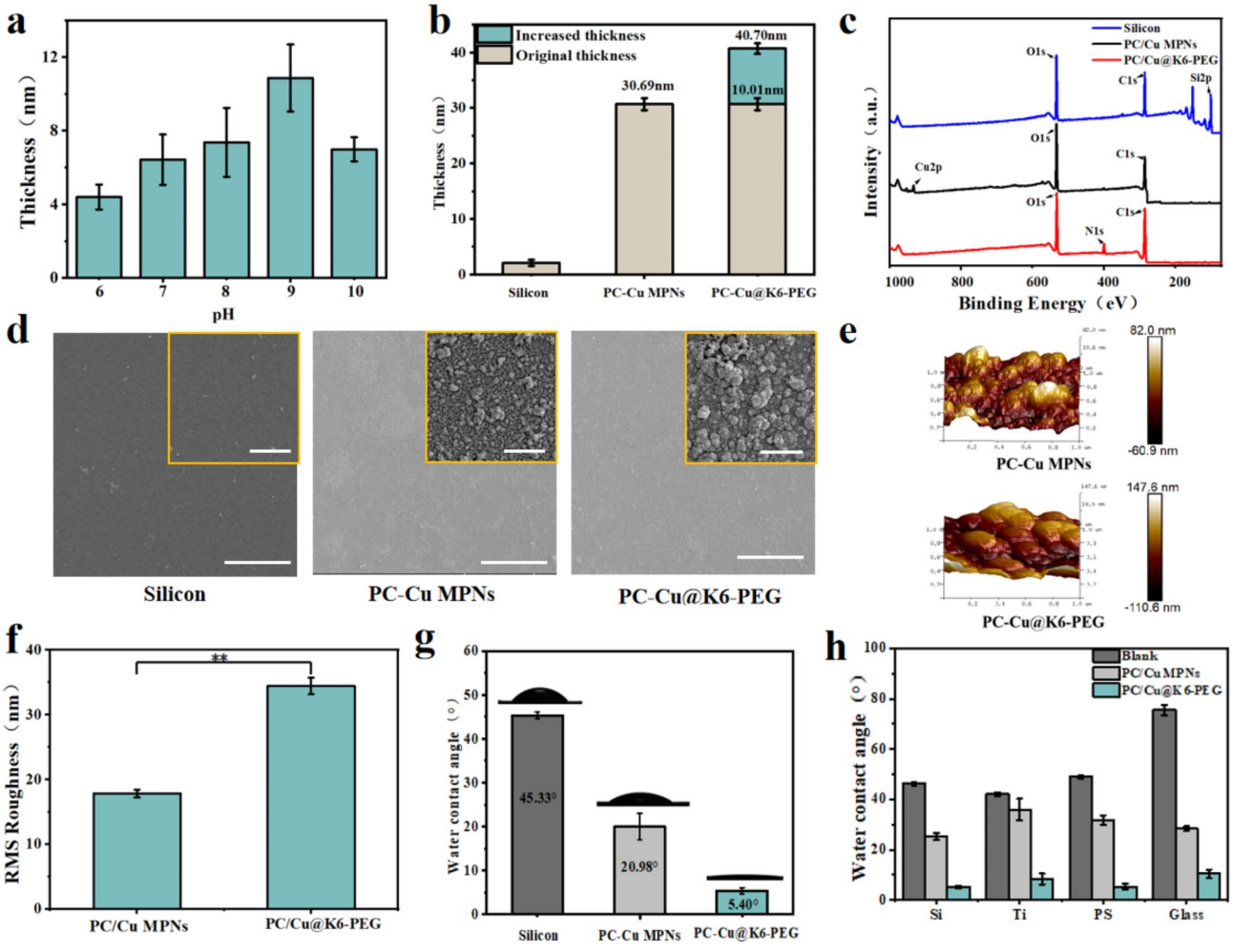

Fig. 2 (**a**) The effect of pH value on the thickness of K6-PEG on PC-Cu MPNs was investigated (PC-Cu MPNs were immersed in K6-PEG (1 mg/ml) solution at pH 6, 7, 8, 9 and10 for 24 h); (**b**) The thickness of PC-Cu MPNs and PC-Cu@K6-PEG (PC-Cu MPNs immersed in K6-PEG (1 mg/ml) for 24 h, pH = 9); (**c**) XPS spectra of the blank silica substrate, PC-Cu MPNs and PC-Cu@K6-PEG; (**d**) SEM images of blank silicon substrates, PC-Cu MPNs coatings, and PC-Cu@K6-PEG coatings; (**e**) Surface morphology and (**f**) Root-mean-square roughness of PC-Cu MPNs and PC-Cu@K6-PEG coatings (measured by AFM); (**g**) Static WCAs of blank silicon substrates, PC-Cu MPNs, and PC-Cu@K6-PEG; (**h**) WCAs of silicon, titanium, glass and plastic substrates before and after PC-Cu MPNs and PC-Cu@K6-PEG coatings. The scale bars in (**d**) were 500 nm and 25 μm

(Fig. 1a). As illustrated in Fig. 2a, the thickness of deposited K6-PEG increased with the increased with the increase in pH of the K6-PEG solution before pH 9, then decreased at pH 9. The pH 9 was selected for the deposition of K6-PEG in the following experiments. At pH 9, the change in coating thickness from 30.69±2.13 nm to 40.70±2.52 nm was observed (Fig. 2b), suggesting an increase of about 10.1 nm after deposition of K6-PEG. In comparison to the PC-Cu MPNs coatings, N1s signals were observed on the PC-Cu@K6-PEG, whereas the nitrogen atoms in the coating are exclusively present in K6 (hexameric lysine), which provides compelling evidence for the successful deposition of K6-PEG (Fig. 2c). The proportion of nitrogen atoms in PC-Cu@K6-PEG was about 8.23%. In contrast, the proportion of Cu atoms in PC-Cu MPNs underwent a notable decline, from 1.98 to 0.19% (Table S1). These findings provide further evidence on the successful deposition of K6-PEG onto MPNs coatings. In order to visualize the morphological changes of the coatings, the coatings were deposited on silicon substrates and observed using a SEM. As illustrated in Fig. 2d, the surface of the PC-Cu MPNs coating appeared to be formed by the successive aggregation of numerous nanoparticles, while larger size was observed after the deposition of K6-PEG. In order to better understand the surface profile, the morphology and roughness of the PC-Cu MPNs and PC-Cu@K6-PEG coatings were examined by AFM. A wavy surface was observed, similar to the morphology observed by SEM, and it can be seen that the particles of the PC-Cu@K6-PEG coatings are larger than those of the PC-Cu MPNs coatings, and not only that, the surface of the PC-Cu@K6-PEG coatings is also wavy (Fig. 2e). In addition, compared to the PC-Cu MPNs coatings, the PC-Cu@K6-PEG coating exhibited a notable alteration in roughness, the root mean square (RMS) roughness increased from 17.84±0.59 nm to 34.46±1.25 nm (Fig. 2f), consistent with the findings by the SEM (Fig. 2d). The WCA was determined before and after K6-PEG deposition, due to the high sensitivity of WCA to surface variations. It was observed that the WCA of the uncoated silicon substrate was 45.33±0.75 °, while the WCA of the surface with PC-Cu MPNs was 20.98±2.98 °. The WCA was further reduced to 5.40±0.2 ° in the following deposition of K6-PEG (Fig. 2g), which strongly supported the successfully deposition of K6-PEG. It is noteworthy that the extremely low WCA of PC-Cu@K6-PEG enables the formation of a robust hydration layer on the surface of the material, which in turn exhibits a high potential to resist biofouling. Furthermore, the coating's ability to be assembled on a range of substrates, including silicon wafers, titanium, glass, and PS plastic, was demonstrated (Fig. 2h), to display the advantage for its wide application. The WCA before and after coating with PC-Cu MPNs or PC-Cu@K6-PEG was measured. The WCA of various substrates with the PC-Cu MPNs coating reduced to 20–30 °, and further significant reduction of the PC-Cu@K6-PEG coated surfaces were observed (<10 ° and even <5 ° for some substrates).

Mechanical properties and hydrophilic ageing of coatings

As an anti-biofouling coating on biomedical devices, it is essential that it maintains good stability under physiological conditions for an extended period of time. Therefore, changes in coating thickness over time were monitored by immersing the PC-Cu@K6-PEG coatings in PBS, 0.9% NaCl solution and cell culture medium DMEM (Fig. 3a). The results showed that there was no significant decrease in the thickness of the PC-Cu@K6-PEG coatings, suggesting that the PC-Cu@K6-PEG coating was stable in the above solution. It has been reported that MPNs lack long-term stability, especially under harsh environment, such as extreme acidic conditions [32], which has limited the application of MPNs. To test whether the introduction of K6-PEG could improve this property, the PC-Cu MPNs coatings and PC-Cu@K6-PEG coatings were subjected to immersion in NaOH (pH=12) and HCl (pH=2) solutions, respectively, for a period of 24 h. As illustrated, both the PC-Cu MPNs and PC-Cu@K6-PEG coatings demonstrated excellent stability in a pH=12 NaOH solution (Fig. 3b). However, at pH 2, the thickness of the PC-Cu MPNs coatings decreased from the initial 30.5±2.31 nm to 15.93±3.05 nm (about 47.74% reduction) within 24 h, a continuous decreasing trend was observed over a 24 h period (Fig. 3c). The PC-Cu@K6-PEG coating exhibited a notable decrease in thickness from 30.5±2.31 nm to 27.77±0.52 nm (a reduction of about 8.92%) within the initial 12 h period, followed by a stabilization phase. These data demonstrated that the deposition of K6-PEG led to a significant enhancement in the acid resistance, compared to the PC-Cu MPNs coating. The Young's modulus and adhesion energy of the coatings were determined by atomic force microscopy (AFM) prior to and following K6-PEG grafting. It can be observed that the Young's modulus of PC-Cu MPNs is 2.41×10^7 Pa, whereas following K6-PEG grafting, the Young's modulus increases to 4.37×10^7 Pa (Fig. 3d), representing a nearly twofold increase. Furthermore, low surface energy is intimately associated with the anti-biofouling capacity of the coating, and anti-biofouling coatings typically exhibit reduced surface adhesion energy [33–35]. As illustrated in Fig. 3e-f, the surface adhesion energy of the coating exhibited a notable decline from 0.0147 N/m to 0.00445 N/m following K6-PEG deposition. For superhydrophilic coatings, the ability to maintain superhydrophilicity over time is crucial for achieving effective anti-biofouling performance. In order to ascertain the impact of UV sterilization on

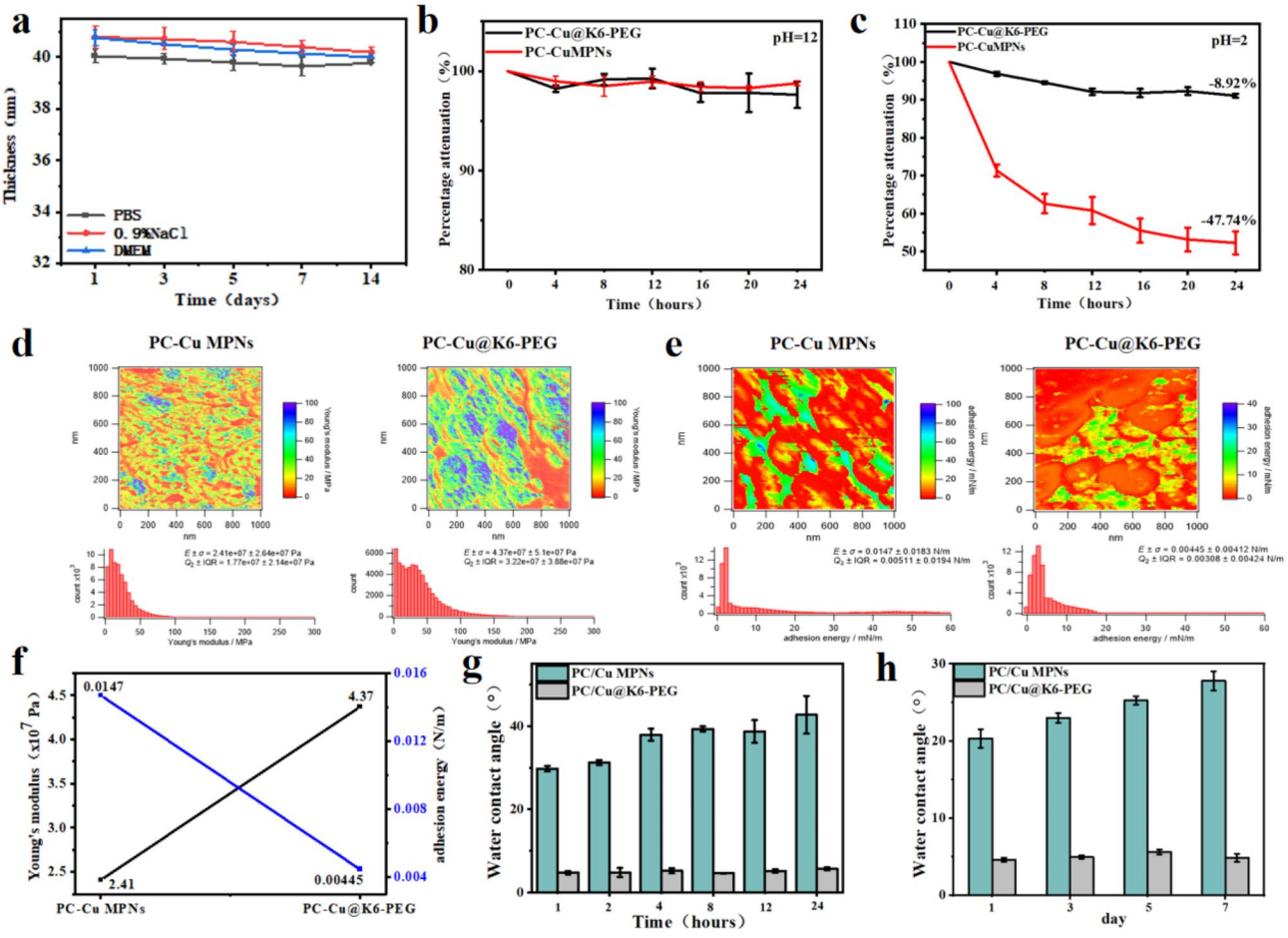

Fig. 3 (**a**) The effect of immersion time on the thickness of the material was investigated for two different solvents: phosphate buffered saline (PBS, 0.9% NaCl) and cell culture medium (DMEM); The ablation of PC-Cu MPNs and PC-Cu@K6-PEG coatings was observed following immersion in solutions with (**b**) pH = 12; (**c**) pH = 2; (**d**) Young's modulus images of coatings in a liquid environment and gaussian distribution of the coated Young's modulus; (**e**) Adhesion energy images of PC-Cu MPNs and PC-Cu@K6-PEG coatings in a liquid environment and gaussian distribution of the coating adhesion energy; (**f**) A comparison of the Young's modulus and adhesion energy of PC-Cu MPNs and PC-Cu@K6-PEG coatings; (**g**) The WCAs of PC-Cu MPNs and PC-Cu@K6-PEG coatings after 1, 2, 4, 8, 12, and 24 h of UV irradiation; (**h**) The WCAs of PC-Cu MPNs and PC-Cu@K6-PEG coatings after 1, 3, 5, and 7 days of immersion in PBS

biomedical applications, the coatings were subjected to UV irradiation. The results demonstrated that there was no notable alteration in the WCA on the coating surface following 24 h of UV irradiation (Fig. 3g). Additionally, no considerable change in the WCA on the coating surface was observed after the coating was immersed in PBS for 7 days (Fig. 3h). These findings suggest that the coating retains its initial superhydrophilicity, which is conducive to long-lasting antifouling performance.

Depositing mechanism of K6-PEG

The fabrication of anti-biofouling polymer brushes represents the primary method of mitigating non-specific adhesion to medical device surfaces. The material composition and structural properties of polymer brushes are of significant relevance to the prevention of biofouling. One of the most crucial aspects is the grafting density of polymer brushes. It has been demonstrated that a high graft density enhance the structural stability, hydration strength (a stronger hydration layer), and resistance to bio-contamination of polymer brushes [36]. A comparison of the grafting densities of the polymer brushes obtained from the aforementioned methods and the present work was illustrated in Fig. 4a [37–42]. The maximum grafting density reported in other documents was 0.79 chains/nm^2 for GF strategy and 1.9 chains/nm^2 for GT strategy. In this work, the calculated graft density of K6-PEG on PC-Cu MPNs was found to be 4.06 chains/nm^2. Given these observations, an investigation was undertaken into the adsorption mechanism of K6-PEG in MPN coatings with a view to elucidating the rationale behind the elevated graft density observed on the coating surface. By blocking one or more of these interactions, it is possible to compare the change in layer thickness of PC-Cu@K6-PEG with that of the MPNs control group, thereby enabling an investigation of the

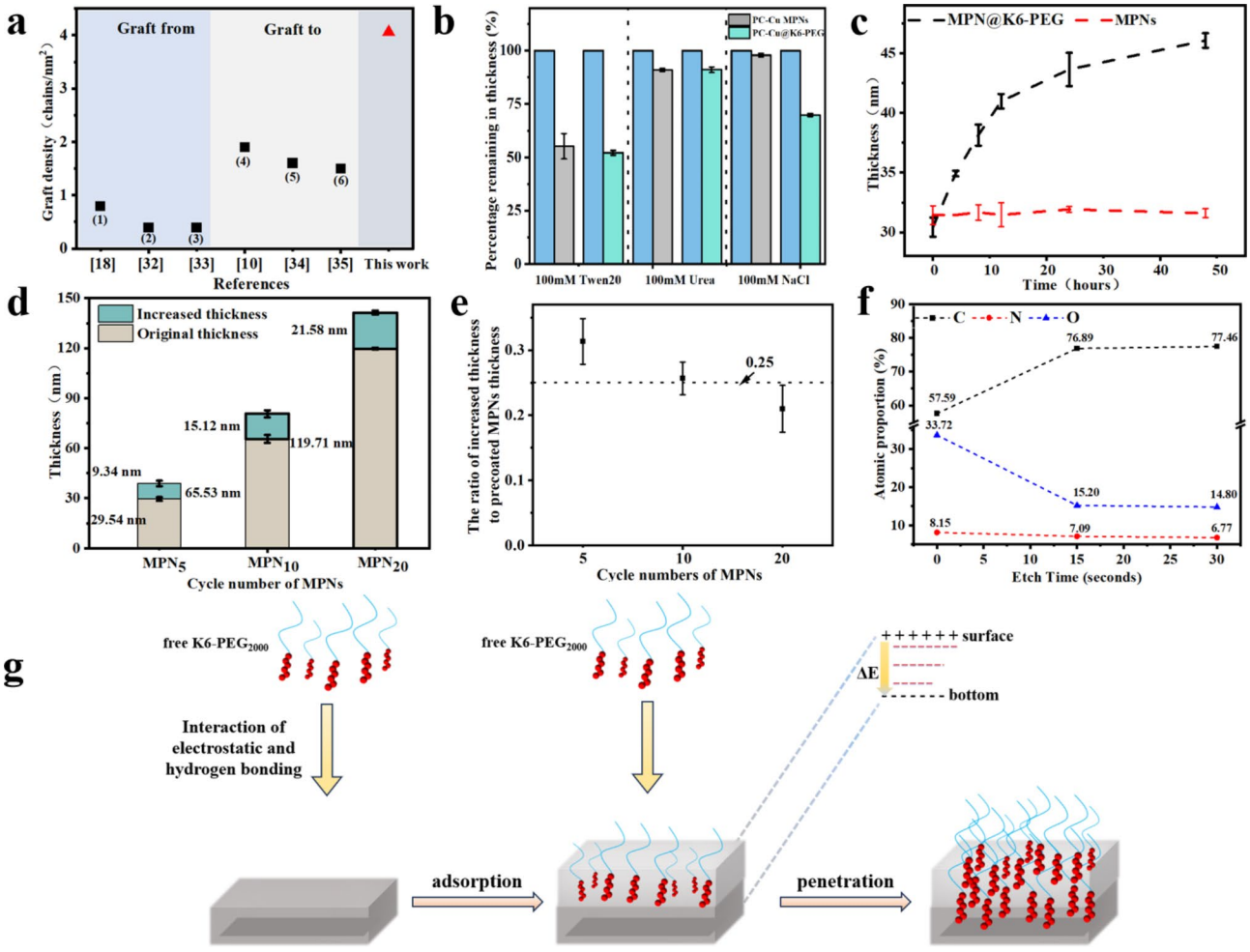

Fig. 4 (**a**) The graft density presented by GF (symbols of (1–3)) and GT (symbols of (4–6)) strategies in previous documents, and this work; (1) PEG brushes formed by surface-initiated aqueous-phase ATRP of methoxypolyethyleneglycol (750) acrylamide ($MPEG_{350}Am$) monomers; (2) and (3) PEG brushes on silicon by surface initiated ATRP of oligo(ethylene glycol) methyl ether methacrylate ($OEGMA_{300}$); (4) PEG layer immobilized on titanium by electrolytic reduction using o-quinone-linked PEG; (5) PEG brushes prepared by adsorption of thiol-ended PEG onto gold surfaces; (6) PEG brushes fixed onto magnetite surface by the coordinative interaction between carboxyl-terminated PEG and iron; (**b**) Percentage remaining of PC-Cu@K6-PEG coatings abated after immersion in 100 mM urea, Tween 20 and NaCl solutions; (**c**) The effect of immersing time into K6-PEG and (**d**) the cycle numbers of PC-Cu MPNs on the thickness of PC-Cu@K6-PEG; (**e**) The ratio of the increased thickness after K6-PEG deposition on MPNs with different cycle numbers to the thickness of the original MPNs; (**f**) Atomic ratios of PC-Cu PC-Cu@K6-PEG after different etch times (15 nm per etch depth with 15 s etching) measured by XPS; (**g**) Scheme of K6-PEG on the penetration process of PC-Cu MPNs

interaction between K6-PEG and MPNs. As illustrated in Fig. 4b, the coatings were immersed in 100 mM Tween 20 (shielded from hydrophobic interaction), 100 mM NaCl (shielded from electrostatic interaction), and 100 mM urea (shielded from hydrogen bonding interaction), respectively. There was essentially no reduction in MPNs in the NaCl solution. In contrast, the desorption rate of PC-Cu@K6-PEG was 30%, suggesting that the deposition process is primarily electrostatically driven. This result was consistent with the dependent deposition of K6-PEG on pH, which was a indication on electrostatic interaction [31]. Furthermore, the deposited thickness of K6-PEG on MPNs is strongly relied on the immersing time (Fig. 4c). It showed very slow depositing process with time, there was no plateau even after the tested 48 h. It was further found that the deposition process was also related to the thickness of the initial MPN. As illustrated in Fig. 4d, for the MPNs with different cycle numbers and thickness of 29.54±1.10 nm, 65.53±2.35 nm, and 119.71±0.57 nm, the increased thicknesses were 9.34±1.61 nm, 15.12±2.09 nm, and 21.58±1.19 nm, respectively, after soaking into K6-PEG solution at pH 9 for 24 h (Fig. 4d). The increased thicknesses attributed to K6-PEG deposition were obtained as 9.34±1.61 nm, 15.12±2.09 nm, and 21.58±1.19 nm for the MPNs respectively. To better observe the contribution of precoated MPNs to the increased thickness, the increased thickness was normalized by the thickness of MPNs, and the data was showed

in (Fig. 4e). It's found that the ratio of increased thickness to the thickness of precoated MPNs was very close to 0.25, meaning per 100 nm precoated MPNs contributed to a 25 nm increase of K6-PEG coating.

The elemental distribution of PC-Cu@K6-PEG at varying depths was subsequently examined through XPS etching. Specifically, the elemental distribution on the surface of PC-Cu@K6-PEG was initially analyzed by XPS. Subsequently, the layer was etched downward once (through a thickness of 15 nm) by XPS, maintaining the original position. Ultimately, the layer was etched downward once more, also through a thickness of 15 nm, by XPS. The results demonstrate that the surface of PC-Cu@K6-PEG films was comprised of 57.59% carbon (C), 8.15% nitrogen (N), and 33.72% oxygen (O) atoms, respectively. Following the initial 15 s of etching, a decrease in the percentage of detected N and O atoms was observed, while the percentage of detected C atoms increased. Following an additional 15 s of etching, the percentage of C, N, and O atoms in the film remained at 76.89%, 7.09%, and 15.20%, respectively (Fig. 4f). As the etching process continues, the proportions of C, N, and O atoms tend to stabilize, with the atomic proportion of the N element remaining at 6.77%. These results strongly indicated that the deposition of K6-PEG occurred not only on the surface but also within the MPN. The deposition process of K6-PEG is proposed in Fig. 4g. Initially, the free K6-PEG in solution is attracted to the MPN by electrostatic and hydrogen bonding interactions, resulting in the adsorption of K6-PEG on the MPN. The positive charge of K6 changed the zeta potential on the MPN surface, thereby creating an electrostatic potential energy difference (ΔE) between the top and bottom of the MPN. In the presence of this negative electric field, the positively charged K6 is further attracted deeper into the MPN until a even distribution of K6-PEG throughout the MPN layer is achieved.

Passivated protein-adsorption properties

Contact of the interventional catheter with blood results in the rapid adsorption of plasma proteins (especially fibrinogen) to the surface of the material, which then undergoes a conceptual transformation to form fibrin. The adsorption and denaturation of proteins can give rise to a number of complications, including acute thrombosis, acute inflammation, and a reduction or loss of the biological function of the surface. Consequently, it is of paramount importance to assess the adsorption properties of proteins on the surface of implant materials [43].

The non-fouling properties of hydrophilic materials are closely related to the hydration layer near the surface. This tightly bound water layer forms a physical and energetic barrier that prevents protein adsorption to the surface [44, 45]. In order to determine the dynamic passivation adsorption capacity of the coatings for different proteins, a series of tests were carried out using a quartz crystal microbalance (Q-CMD) to assess the adsorption of PC-Cu MPNs and PC-Cu@K6-PEG coatings for a range of proteins. Proteins with disparate physicochemical properties (including molecular weight (Mw) and isoelectric point (IP)) were selected for investigation (BSA has a molecular weight of 68 KD and IP 4.8; Lys has a molecular weight of 14–15 KD and IP 10.5–11.0; fibrinogen has a molecular weight of 330–340 KD and an IP 5.5; haemoglobin has a molecular weight of 67 KD and IP 4.5-5.0; and mucin has a molecular weight of 110 KD and IP 3.0–5.0). Specifically, 1 mg/ml BSA, Lys, fibrinogen, haemoglobin and mucin were dissolved in 1X PBS (pH=7.4), the gold coated sensor was mounted in a Q-CMD chamber, the peristaltic pump speed was 90 rpm and the system temperature was set at 25 ℃ PBS was then passed through until the curves became smoother and then the PBS was changed to the protein solutions above. As illustrated in Fig. 5a-e, the time-dependent resonance frequencies on the gold sensor surface demonstrated that proteins were adsorbed by flowing on the material surface. In comparison to the PC-Cu MPNs group, the PC-Cu@K6-PEG coating group exhibited a significantly reduced change in frequency (6–9 times lower). In addition, the mass of proteins adsorbed on the surface of the gold sensor was calculated using the equation under the viscoelastic model, and the blank control group adsorbed the most amount of proteins on the surface up to 1,235.32 ng/cm^2, while the amount of proteins adsorbed on the PC-Cu@K6-PEG was significantly reduced down to a minimum of 4.09 ng/cm^2 (Fig. 5f), and the anti-adsorption efficiency against proteins was 99.67%. These results indicate that the PC-Cu@K6-PEG coating has good antiadsorption properties for proteins with a wide spectral range.

Furthermore, in order to more effectively illustrate the coating's capacity to resist protein adsorption, the samples were incubated with 1 mg/mL of fluorescein isothiocyanate-labeled bovine serum proteins (FITC-BSA) and lysozyme (FITC-Lys) for a period of 24 h. This allowed for a qualitative and semi-quantitative examination of the static adsorption behaviours of proteins on the surface of the materials. As shown in Fig. 5g, a large amount of fluorescent protein adsorbed on the blank glass slice (control), resulting in high surface fluorescence intensity. In contrast, there was slight decrease fluorescent signal on the PC-Cu MPN coatings and almost no visible fluorescent signal on PC-Cu@K6-PEG coating. From the quantitative analysis in the mean fluorescence (Fig. 5h), the amount of fluorescence adsorbed on the surface of the PC-Cu@K6-PEG coating was significantly reduced, with a fluorescence intensity of 0.5 a.u, which was reduced by a factor of ~150 compared to that of the PC-Cu MPNs and by a factor of ~200 compared to the blank glass

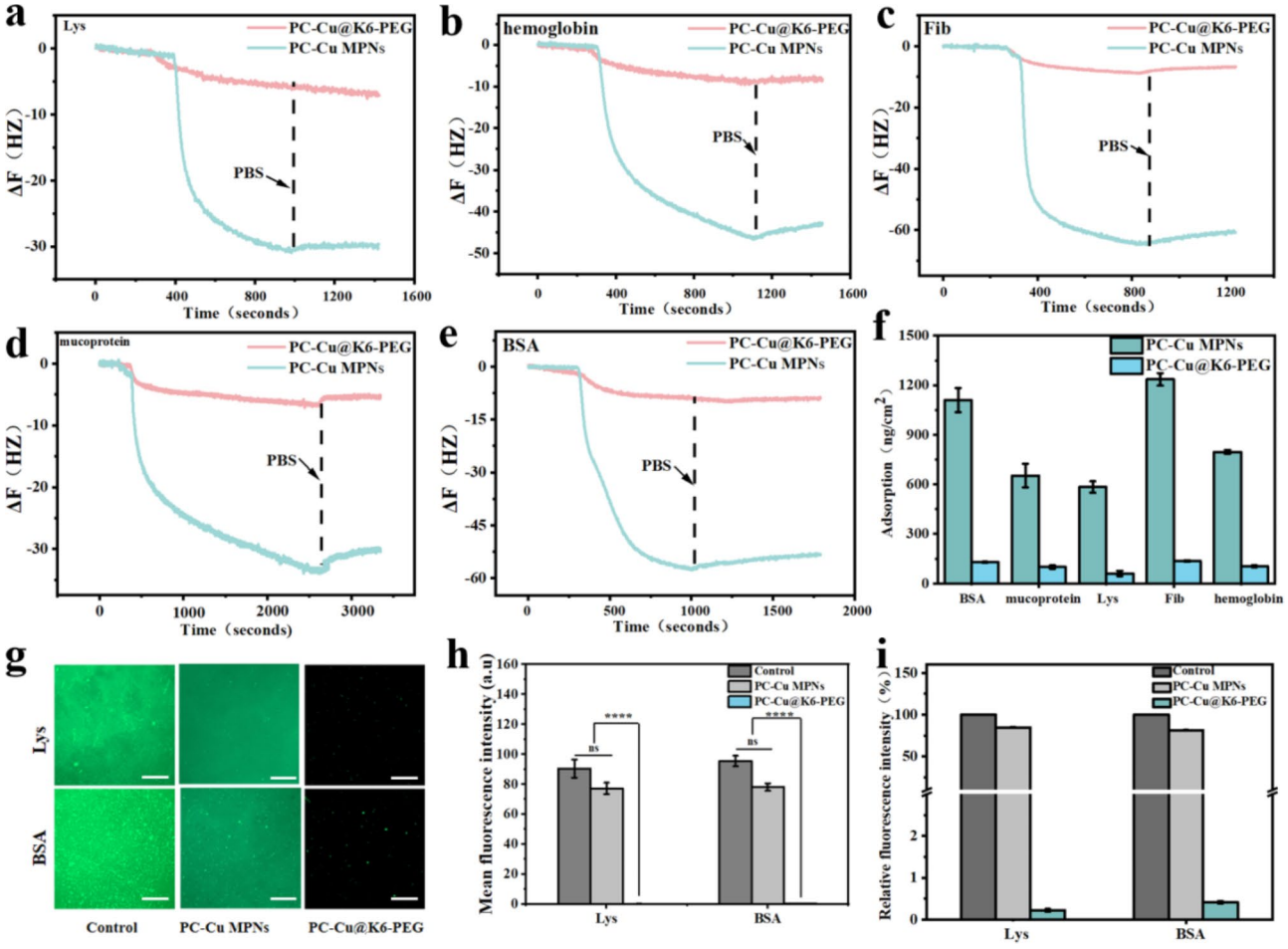

Fig. 5 In QCM-D, the plots of time-dependent resonance frequencies after the adsorption of (**a**) Lys, (**b**) hemoglobia, (**c**) Fib, (**d**) mucoprotein and (**e**) BSA on PC-Cu MPNs and PC-Cu@K6-PEG coatings; (**f**) The quantity of the above adsorbed proteins on the PC-Cu MPNs and PC-Cu@K6-PEG coatings determined by Equations under the viscoelastic model; (**g**) Confocal images of FITC-BSA and FITC-Lys adsorbed on glass (control) the PC-Cu MPNs and PC-Cu@K6-PEG coatings; (**h**) The mean fluorescent intensity and (**i**) relative fluorescent intensity of adsorbed FITC-BSA and FITC-Lys on glass (control) the PC-Cu MPNs and PC-Cu@K6-PEG coatings, as obtained from (**g**). The scale bars in (**g**) were 20 μm. ($N = 3$, no significance noted as "ns", $^{*}p < 0.05$, $^{**}p < 0.01$, $^{***}p < 0.001$ using t-test.)

(control). Figure 5i illustrated the relative fluorescence intensities by normalizing the samples' intensity with the control's, in which a reduced relative fluorescence intensity on PC-Cu MPN coating and significant reduction on PC-Cu@K6-PEG coating was observed. These results suggested that the coating had a strong passivation effect on protein adsorption.

Reduction in bacterial adhesion behaviour

Previous studies have demonstrated that a significant proportion of bacteria contain a variety of protein appendages that play a direct or indirect role in adhesion [46], such as flagella, hyphae, and coils [47–49]. Bacterial adhesion is typically divided into three stages, commencing with reversible initial adhesion. This is followed by a transition to enhanced irreversible adhesion, and finally the development of a mature biofilm [50, 51]. Consequently, the inhibition of initial bacterial adhesion represents a pivotal strategy for the prevention of biofilm formation. The initial 8 h following bacterial contact with the surface is regarded as the "decisive period" for the prevention of bacterial adhesion. Consequently, the samples were incubated with Staphylococcus aureus (*S. aureus*) and Escherichia coli (*E. coli*) for 8 h in order to investigate their resistance to bacteria. Following an eight hours incubation period, the bacteria were stained with a LIVE/DEAD BacLight bacterial viability kit (Steps provided by supplier) and observed under a fluorescence microscope (Fig. 6a). It was observed that severe *E. coli* and *S. aureus* adhesion occurred on blank glass slice group (control) and the PC-Cu MPNs group. In contrast, only a few *E. coli* and *S. aureus* adhesion were observed on the surface of the PC-Cu@K6-PEG sample. A semi-quantitative fluorescence analysis (Fig. 6b) showed that the fluorescence intensity of the PC-Cu MPNs group was slightly reduced (by about two-fold) compared to

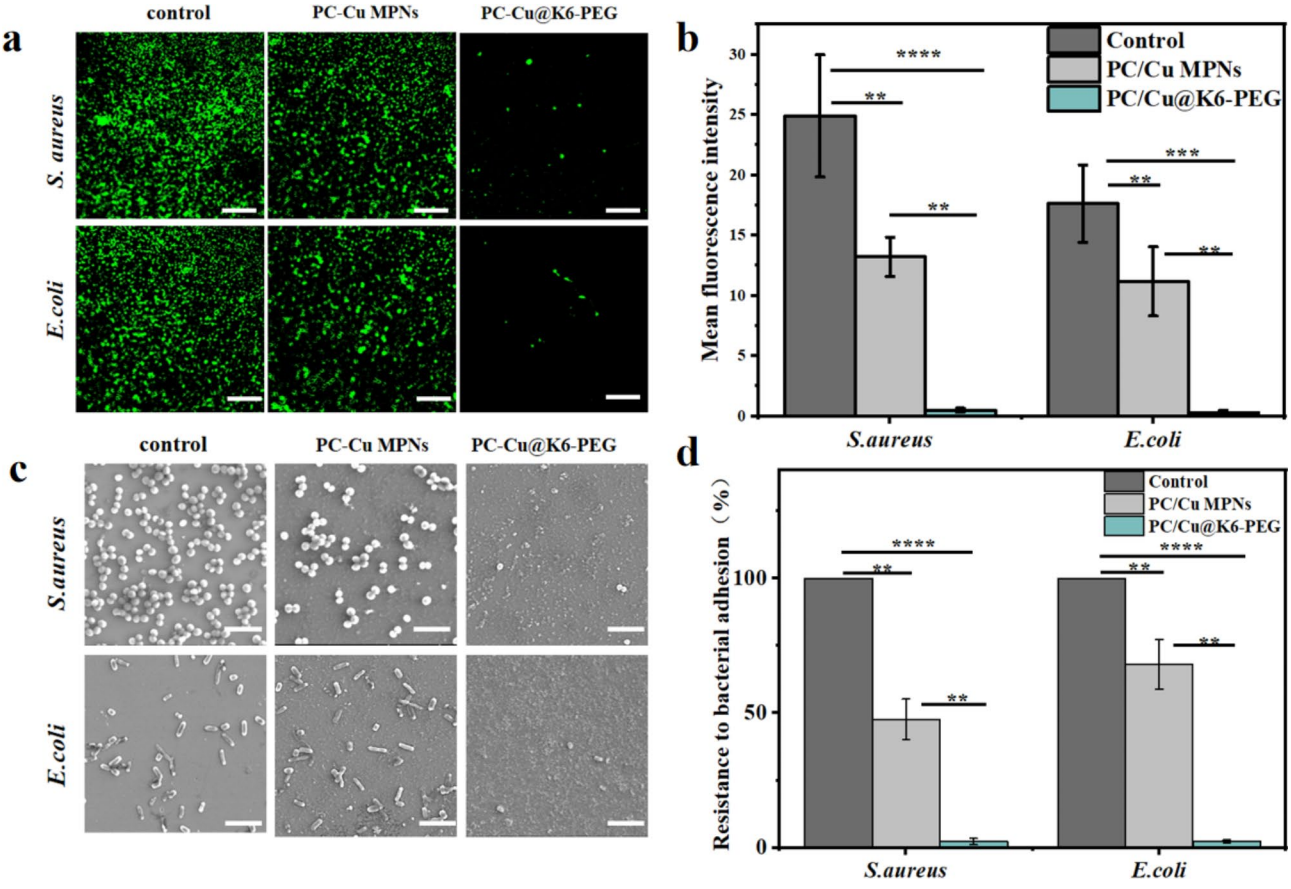

Fig. 6 (**a**) Laser confocal imaging of live-dead-stained *S.aureus* and *E.coli* colonized on blank substrates, PC-Cu MPNs coating and PC-Cu@K6-PEG coating; (**b**) fluorescence semi-quantitative results for them; (**c**) The colonization behavior of Staphylococcus aureus and Escherichia coli on blank substrates, PC-Cu MPNs coatings, and PC-Cu@K6-PEG coatings; (**d**) the counting of their numbers were observed by SEM. The data was statistically derived from the number of bacteria adhering to the surface of the sample ($n=3$). The scale bars in (**a**) were 5 μm and in (**c**) were 2 μm. ($N=3$, no significance noted as "ns", $^{*}p<0.05$, $^{**}p<0.01$, $^{***}p<0.001$ using t-test.)

the blank glass slides, whereas the average fluorescence intensity of the PC-Cu@K6-PEG group was reduced by about 50 folds compared to that of the blank glass slides group, and by about 25 folds compared to that of the PC-Cu MPNs. To provide a more visual representation of the coating's resistance to bacterial adhesion, the incubated bacteria were dehydrated and cured, and then observed for bacterial adhesion on the sample surface by SEM. As illustrated in Fig. 6c, a considerable number of bacteria adhered to the wafer substrate (control group). In contrast, the number of bacteria on the surface of PC-Cu MPNs was relatively reduced, while a significant reduction in bacterial adherence was observed on the surface of PC-Cu@K6-PEG. Furthermore, the quantitative analysis results (Fig. 6d) demonstrated the number of bacterial adhesions was slightly reduced in the PC-Cu MPNs group compared to the control (by about twofold), whereas the number of bacterial adhesions on the PC-Cu@K6-PEG group was reduced by about 100 folds compared to the control group and by about 50 folds compared to the PC-Cu MPNs. The results were attributed to the strong hydrophilicity of PEG in PC-Cu@K6-PEG, which formed a tenacious hydration layer that could strongly repel bacteria when they approached the surface for adhesion [52]. Furthermore, Tanaka et al. [53] proposed the "intermediate water concept" to elucidate the water-mediated repulsion. This concept posits that the physical barrier of intermediate water plays a pivotal role in preventing the adsorption of proteins onto the substrate [50]. The dense intermediate hydration layer formed by the high density of PEG chains on the surface of the coatings successfully prevented the adhesion of bacteria and proteins on the surface. Together, these results demonstrate that the surface-modified PC-Cu@K6-PEG coatings are highly resistant to the adhesion of proteins and bacteria.

Hemolysis and antiplatelet adhesion

One of the most crucial criteria for the successful application of blood-contacting materials and devices is their blood compatibility. This is primarily assessed through in vitro analyses that examine the adhesion of blood

cells and the formation of blood clots [54–56]. The Triton X-100 and 0.9% NaCl solution were employed as the positive and negative controls, respectively. Following incubation with erythrocytes at 37 °C for 4 h (Fig. 7a), the hemolysis rate was found to be less than 5% for both the PC-Cu MPNs coating and the PC-Cu@K6-PEG coating. This indicates that the coatings have a low hemolytic potential. It is well established that platelet adhesion to the surface of biomaterials can trigger blood coagulation and thrombosis [51, 57], The degree of platelet deformation and the amount of platelet adhesion are commonly employed as indicators of hemocompatibility in biomaterials [58, 59]. To assess the resistance of samples to platelet adhesion, platelet adhesion tests were carried out using SEM to observe their morphology as well as quantitative analysis by counting the number of adherent platelets. As shown in Fig. 7b, there was a significant difference in the degree of platelet adhesion on the surface of the different samples, with A large number of platelets adhered to the blank silicon substrate (control) (approximately 30,000/cm^2), and a relatively small number of platelets (approximately 10,000/cm^2) adhered to the PC-Cu MPN surface. In contrast, the presence of K6-PEG enabled the coating to effectively inhibit platelet adhesion and aggregation with a value of less than 50 / cm^2, and the reduction of platelet adhesion was about 99.84%. Normalised to the number of platelets adhering to the surface of the control samples in Fig. 7b, as shown in Fig. 7c, we can see that the number of platelets adhering to the surface of the PC-Cu MPNs coatings differs from that of the control group by only one star, while the PC-Cu@K6-PEG group shows a significantly smaller difference than the latter group. These data suggest PC-Cu@K6-PEG coating exhibited considerable antithrombotic potential.

In addition, in order to illustrate more the performance of PEG brushes with high graft density in anti-biofouling, the results of this study were compared with those of other studies (Table S2). It can be seen that in the GT's strategy, the highest graft density PEG brushes achieved 98.93% anti-sorption of bovine serum proteins and 99% anti-adhesion of platelets. In the strategy of GF, the PEG brush with the highest graft density achieved 90% antisorption of human serum proteins and more than 99.5% antiadhesion to platelets. In the present study, antisorption of lysozyme, bovine serum proteins, fibrinogen, mucin, and hemoglobin were studied, with a maximum antisorption effect of 99.7% and an antimutagenic effect

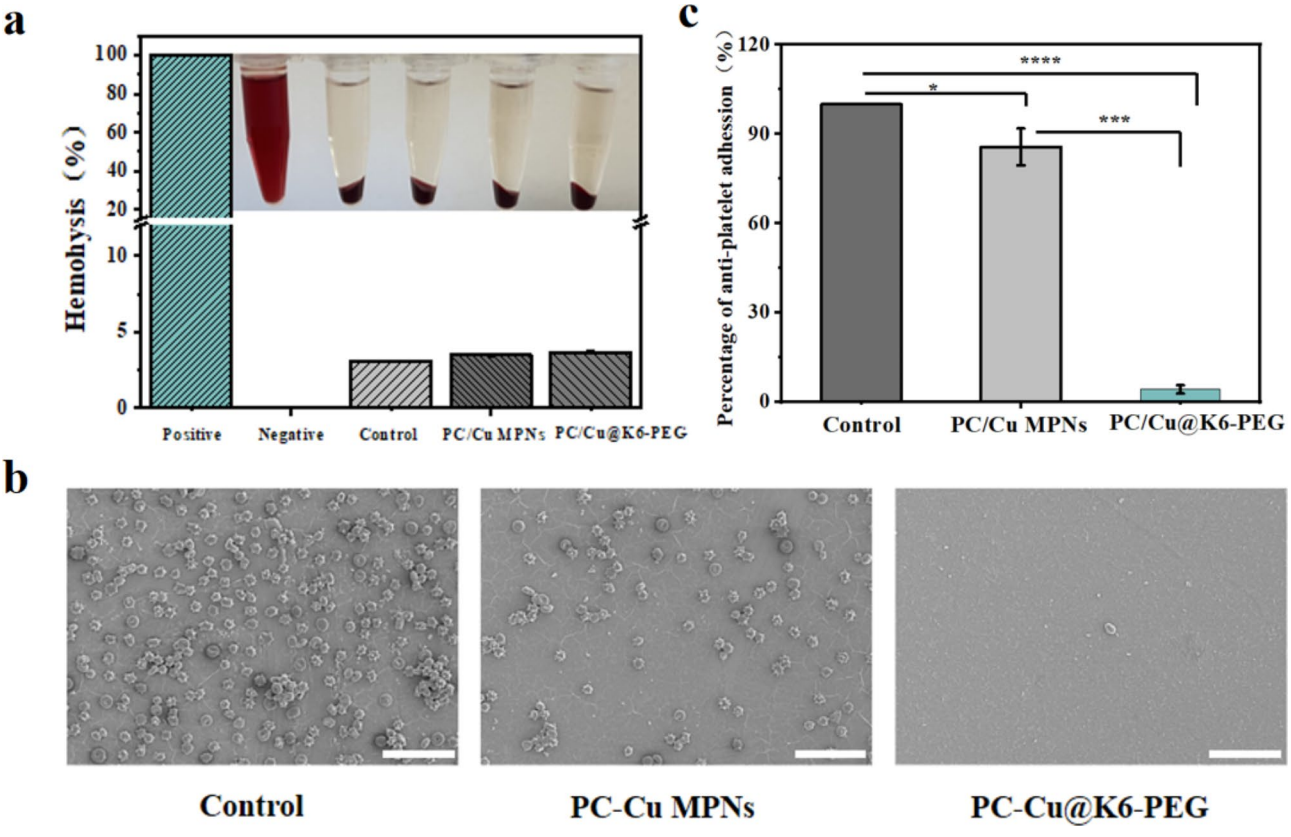

Fig. 7 (**a**) Hemolysis test of red blood cells of blank silicon substrate, PC-Cu MPNs and PC-Cu@K6-PEG coatings; (**b**) SEM images of platelets adhering to bare and modified polyurethane. (**c**) Platelet adhesion rate normalised to the number of platelets in the control group in figure b. The scale bars in (**b**) were 20 µm. ($N = 3$, no significance noted as "ns", *$p < 0.05$, **$p < 0.01$, ***$p < 0.001$ using t-test.)

of more than 99.8% on platelets (see Table S2 for more comparisons).

Ex vivo antithrombogenic properties

In order to further simulate clinical applications, in vitro catheter blood circulation experiments were conducted [60]. Rabbit arteriovenous shunt circuits were connected using commercially available medical polyurethane catheters with different surface treatments. (Fig. 8a) Following 2 h of ex vivo flow circulation without any systemic heparin anticoagulation, thrombus formation was found to be slightly reduced in the PC-Cu MPNs group in comparison with the catheter without coatings (Fig. 8b). Almost no obvious thrombus formation was observed in the PC-Cu@K6-PEG group. SEM analysis additionally demonstrated that the grafting of K6-PEG effectively inhibited thrombus formation (Fig. 8c). The blood-contact surfaces of bare PU and PU-MPNs tubes showed severe thrombosis with properties of densely interconnected polymerized fibrin networks, red blood cells, and activated platelets, in the PU-PC-Cu@K6-PEG group, only a very small number of haemocytes were seen on the surface (Fig. 8c). Quantitative analysis of these results further showed that thrombosis was significantly reduced in the PC-Cu@K6-PEG group compared to the other groups, as evidenced by the assessment of thrombus weight, occlusion rate (Fig. 8d-e). Specifically, PC-Cu@K6-PEG showed an approximately 30 folds and 21 folds reduction in mean clot weight compared with the PU tubing group and the PC-Cu MPNs group, respectively (Fig. 8d) Furthermore, the catheter occlusion rate was quantified by calculating the percentage of lumen area occlusion using computerised image analysis (Fig. 8e). The PC-Cu@K6-PEG modified catheters exhibited a significant reduction in thrombus occlusion rate compared to the PU tube group and PC-Cu MPNs group, with an occlusion rate of approximately 5%. These results clearly demonstrated that the K6-PEG modification imparts excellent anti-thrombotic properties to the material surface.

The two main factors involved in thrombosis on blood contact implants are fibrinogen (Fib) adsorption and activation and platelet adhesion and activation [61]. Preliminary experiments confirmed the anti-absorptive capacity of the K6-PEG-modified surface against a wide range of proteins (including Fib, hemoglobia, etc.), as well as its resistance to platelet adhesion, suggesting a potential anti-thrombotic capacity. This was subsequently confirmed by the results of in vitro blood circulation experiments in rabbits. Therefore, the PC-Cu@K6-PEG coating has good prospects for use in medical antithrombotic catheters.

Conclusions

In summary, the coating with strong resistance to non-specific protein adsorption, PC-Cu@K6-PEG, was successfully engineered through direct depositing K6-PEG onto pre-constructed PC-Cu MPNs. The introduction of

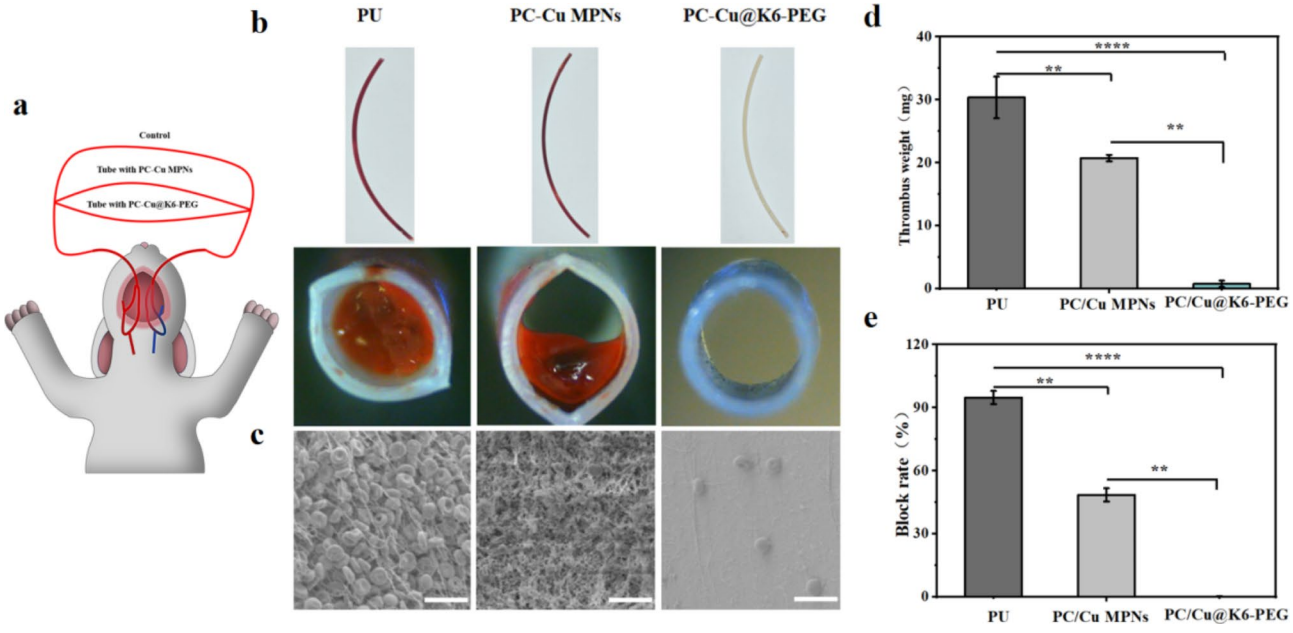

Fig. 8 (**a**) Schematic illustration of arteriovenous (AV) shunt model connected to the rabbit; (**b**) Photographs of side (top) and cross-section (bottom) view of the bare and modified PU tubes after blood circulation; (**c**) Lumen surface morphology of each sample after blood circulation characterized by SEM; (**d**) thrombus quality; (**e**) catheter masking ratio.The scale bars in (**c**) were 20 μm. ($N = 3$, no significance noted as "ns", *$p < 0.05$, **$p < 0.01$, ***$p < 0.001$ using t-test.)

K6-PEG into MPN has been demonstrated to improve both the stability and the mechanical properties of PC-Cu MPN, while simultaneously reducing the contact angle and adhesion energy of PC-Cu. K6-PEG is able to penetrate throughout PC-Cu MPNs, resulting in the formation of PC-Cu@K6-PEG with an ultrahigh PEG grafting density (4.06 chains/nm^2). The deposition of K6-PEG to PC-Cu showed significantly reducing the adsorption of a variety of proteins (Lys; hemoglobia; Fib; mucoprotein; BSA) and bacteria (*E. coli* and *S. aureus*). Ex vivo blood circulation test demonstrated that PC-Cu@K6-PEG significantly reduced platelet adhesion on the surface of implanted catheters and prevented thrombus formation. It should be highlighted that the preparation of PC-Cu@K6-PEG coatings is a straightforward and environmentally friendly process that can be applied to a wide variety of substrates without any limitations in terms of material or shape, we believe this strategy offers a promising avenue for the development of anti-biofouling coating applications. In future studies, we envision that by changing the molecular weight of the PEG or by changing the structure of the PEG chain to obtain a defect-free surface of the PEG brushes, a complete anti-biofouling effect can be achieved.

Supplementary Information

The online version contains supplementary material available at https://doi.org/10.1186/s12951-024-03026-x.

Supplementary Material 1

Acknowledgements
Thanks for the Wenzhou Municipal Bureau of Science and Technology (Y20240088) and the Wenzhou Institute of the Chinese Academy of Sciences (WIUCASQD2021043) for funding this work. Thank you to the following contributors: Wenjie Liu: Experimental work, data Formal analysis, manuscript writing; Hao Liu: Experimental work, data Formal analysis; Zeyu Shou: Experimental work, data Formal analysis; Kaiyuan Huo, Hongping Xiang, Aihan Feng: data Formal analysis; Suqin He, Wei Lu: Conception and design; Na Li: Conception and design, data Formal analysis, manuscript writing.

Author contributions
Wenjie Liu: Experimental work, data Formal analysis, manuscript writing; Hao Liu: Experimental work, data Formal analysis; Zeyu Shou: Experimental work, data Formal analysis; Kaiyuan Huo, Hongping Xiang, Aihan Feng: data Formal analysis; Suqin He, Wei Lu: Conception and design; Na Li: Conception and design, data Formal analysis, manuscript writing.

Funding
Not applicable.

Data availability
No datasets were generated or analysed during the current study.

Declarations

Ethics approval and consent to participate
Not applicable.

Consent for publication
All authors declare full consent for publication.

Competing interests
The authors declare no competing interests.

Author details
[1]School of Materials Science and Engineering, Zhengzhou University, Zhengzhou 450001, Henan, China
[2]Wenzhou Institute, University of Chinese Academy of Sciences, Wenzhou Key Laboratory of Perioperative Medicine, Wenzhou 325001, Zhejiang, China
[3]Department of Orthopedics, The First Affiliated Hospital of Wenzhou Medical University, Wenzhou 325000, Zhejiang, China
[4]Shanghai Key Laboratory of D&A for Metal-Functional Materials, School of Materials Science & Engineering, Tongji University, Shanghai 201804, China
[5]Department of Cardiovascular Surgery, The Quzhou Afliated Hospital of Wenzhou Medical University, Quzhou People's Hospital, Quzhou 32400, Zhejiang, China

Received: 27 September 2024 / Accepted: 19 November 2024
Published online: 02 December 2024

References

1. Bekmurzayeva A, Duncanson WJ, Azevedo HS, Kanayeva D. Surface modification of stainless steel for biomedical applications: revisiting a century-old material. Mater Sci Eng C-Materials Biol Appl. 2018;93:1073–89.
2. Cao H, Zhu T, Wei H, Zhang S. Poly(sulfobetaine) versus poly(ethylene glycol) based copolymer modified polyurethane catheters for antifouling. J Mater Chem B. 2024;12:5455–64.
3. Ren Y, Zhou H, Lu J, Huang S, Zhu H, Li L. Theoretical and experimental optimization of the Graft density of Functionalized Anti-biofouling surfaces by Cationic Brushes. Membranes 2020, 10.
4. Zhang Y, Zhang L, Duan S, Hu Y, Ding X, Zhang Y, Li Y, Wu Y, Ding X, Xu F-J. Heparinized anticoagulant coatings based on polyphenol-amine inspired chemistry for blood-contacting catheters. J Mater Chem B. 2022;10:1795–804.
5. Parada G, Yu Y, Riley W, Lojovich S, Tshikudi D, Ling Q, Zhang Y, Wang J, Ling L, Yang Y et al. Ultrathin and Robust Hydrogel Coatings on Cardiovascular Medical Devices to mitigate thromboembolic and infectious complications. Adv Healthc Mater 2020, 9.
6. Fan BE, Cui NF, Xu ZW, Chen K, Yin PC, Yue K, Tang W. Thermoresponsive and Self-Healing Hydrogel based on Chitosan Derivatives and polyoxometalate as an Antibacterial Coating. Biomacromolecules. 2022;23:972–82.
7. Yebra DM, Kiil S, Dam-Johansen K. Antifouling technology - past, present and future steps towards efficient and environmentally friendly antifouling coatings. Prog Org Coat. 2004;50:75–104.
8. Zhao CW, Zhou L, Chiao M, Yang WT. Antibacterial hydrogel coating: strategies in surface chemistry. Adv Colloid Interface Sci. 2020;285:17.
9. Leslie DC, Waterhouse A, Berthet JB, Valentin TM, Watters AL, Jain A, Kim P, Hatton BD, Nedder A, Donovan K, et al. A bioinspired omniphobic surface coating on medical devices prevents thrombosis and biofouling. Nat Biotechnol. 2014;32:1134–40.
10. Pereira AS, Sheikh S, Blaszykowski C, Pop-Georgievski O, Fedorov K, Thompson M, Rodriguez-Emmenegger C. Antifouling polymer brushes displaying Antithrombogenic Surface properties. Biomacromolecules. 2016;17:1179–85.
11. Shin E, Lim C, Kang UJ, Kim M, Park J, Kim D, Choi W, Hong J, Baig C, Lee DW, Kim B-S. Mussel-inspired Copolyether Loop with Superior Antifouling Behavior. Macromolecules. 2020;53:3551–62.
12. Liu S, Chen L, Tan L, Cao F, Bai L, Wang Y. A high efficiency approach for a titanium surface antifouling modification: PEG-o-quinone linked with titanium via electron transfer process. J Mater Chem B. 2014;2:6758–66.
13. van Andel E, Lange SC, Pujari SP, Tijhaar EJ, Smulders MMJ, Savelkoul HFJ, Zuilhof H. Systematic comparison of Zwitterionic and Non-zwitterionic Antifouling Polymer brushes on a bead-based platform. Langmuir. 2019;35:1181–91.
14. Buzzacchera I, Vorobii M, Kostina NY, Pereira AS, Riedel T, Bruns M, Ogieglo W, Moeller M, Wilson CJ, Rodriguez-Emmenegger C. Polymer brush-functionalized Chitosan Hydrogels as Antifouling Implant Coatings. Biomacromolecules. 2017;18:1983–92.
15. Zoppe JO, Ataman NC, Mocny P, Wang J, Moraes J, Klok H-A. Surface-initiated controlled radical polymerization: state-of-the-Art, opportunities, and challenges in Surface and Interface Engineering with Polymer brushes. Chem Rev. 2017;117:1105–318.

16. Horiguchi Y, Nakayama N, Kanayama N, Nagasaki Y. Sulfobetaine-terminated PEG improves the qualities of an immunosensing surface. Biomaterials Sci 2014, 2.
17. Yoshimoto K, Nozawa M, Matsumoto S, Echigo T, Nemoto S, Hatta T, Nagasaki Y. Studies on the Adsorption Property and structure of polyamine-ended poly(ethylene glycol) derivatives on a gold surface by Surface Plasmon Resonance and Angle-resolved X-ray Photoelectron Spectroscopy. Langmuir. 2009;25:12243–9.
18. Yoshimoto K, Hirase T, Nemoto S, Hatta T, Nagasaki Y. Facile construction of sulfanyl-terminated poly(ethylene glycol)-brushed layer on a gold surface for protein immobilization by the combined use of sulfanyl-ended telechelic and semitelechelic poly(ethylene glycol)s. Langmuir. 2008;24:9623–9.
19. Chiu CY, Chang Y, Liu TH, Chou YN, Yen TJ. Convergent charge interval spacing of zwitterionic 4-vinylpyridine carboxybetaine structures for superior blood-inert regulation in amphiphilic phases. J Mater Chem B. 2021;9:8437–50.
20. Dalsin JL, Lin LJ, Tosatti S, Vörös J, Textor M, Messersmith PB. Protein resistance of titanium oxide surfaces modified by biologically inspired mPEG-DOPA. Langmuir. 2005;21:640–6.
21. Dalsin JL, Hu BH, Lee BP, Messersmith PB. Mussel adhesive protein mimetic polymers for the preparation of nonfouling surfaces. J Am Chem Soc. 2003;125:4253–8.
22. Cole M, Voelcker NH, Thissen H. Switchable coatings for biomedical applications. In *Conference on Biomedical Applications of Micro- and Nanoengineering II*; 2005 *Dec 13–15*. 2004: 19–27.
23. izhakkedathu JNJJ, Le Y, et al. Poly (oligo (ethylene glycol) acrylamide) brushes by surface initiated polymerization effect of macromonomer chain length on brush growth and protein adsorption from blood plasma. Langmuir. 2009;25(26):3794–801.
24. F AND T-Wang Y-M, Kalosi A, Halahovets Y, Romanenko I, Slaby J, Homola J, Svoboda J, Pereira AdlS, Pop-Georgievski O. Grafting density and antifouling properties of poly[N-(2-hydroxypropyl) methacrylamide] brushes prepared by grafting to and grafting from. Polym Chem. 2022;13:3815–26.
25. Ejima H, Richardson JJ, Liang K, Best JP, van Koeverden MP, Such GK, Cui JW, Caruso F. One-step assembly of Coordination complexes for Versatile Film and Particle Engineering. Science. 2013;341:154–7.
26. Li XY, Gao P, Tan JY, Xiong KQ, Maitz MF, Pan CJ, Wu HK, Chen Y, Yang ZL, Huang N. Assembly of Metal Phenolic/Catecholamine Networks for synergistically anti-inflammatory, antimicrobial, and Anticoagulant Coatings. ACS Appl Mater Interfaces. 2018;10:40844–53.
27. Long L, Fan Y, Yang X, Ding X, Hu Y, Zhang G, Xu F-J. A hydrophobic cationic polyphenol coating for versatile antibacterial and hemostatic devices. Chem Eng J 2022, 444.
28. Shou Z, Bai Z, Zhou H, Shen Y, Huang X, Meng H, Xu C, Wu S, Li N, Chen C. Engineering tunable dual peptide hybrid coatings promote osseointegration of implants. Mater Today Bio 2024, 24.
29. Zhao B, Dong Y, Shen X, He W, Jin H, Yao L, Zheng S, Zan X, Liu J. Construction of multifunctional coating with cationic amino acid-coupled peptides for osseointegration of implants. Mater Today Bio 2023, 23.
30. Hai MT, Magdassi S. Investigation on the release of fluorescent markers from w/o/w emulsions by fluorescence-activated cell sorter (96, pg 393, 2004). J Controlled Release. 2004;97:383–383.
31. Li N, Shou Z, Liu W, Huo K, Liu H, Zan X, Zhan Y, Hu S. A strategy of de novo peptides for customizing supramolecular self-assembly coating with desired biological functionalities. Chem Eng J 2024, 496.
32. Cheng X, Lu R, Zhang X, Zhu Y, Wei S, Zhang Y, Zan X, Geng W, Zhang L. Silanization of a metal-polyphenol coating onto Diverse substrates as a strategy for controllable wettability with enhanced performance to Resist Acid Corrosion. Langmuir. 2021;37:3637–47.
33. Hu P, Xie Q, Ma C, Zhang G. Fouling resistant silicone coating with self-healing induced by metal coordination. Chem Eng J 2021, 406.
34. Hu P, Xie R, Xie Q, Ma C, Zhang G. Simultaneous realization of antifouling, self-healing, and strong substrate adhesion via a bioinspired self-stratification strategy. Chem Eng J 2022, 449.
35. Boo C, Hong S, Elimelech M. Relating Organic fouling in membrane distillation to Intermolecular Adhesion Forces and Interfacial Surface energies. Environ Sci Technol. 2018;52:14198–207.
36. Song X, Man J, Qiu Y, Wang J, Liu J, Li R, Zhang Y, Li J, Li J, Chen Y. High-density zwitterionic polymer brushes exhibit robust lubrication properties and high antithrombotic efficacy in blood-contacting medical devices. Acta Biomater. 2024;178:111–23.
37. Feng W, Gao X, McClung G, Zhu S, Ishihara K, Brash JL. Methacrylate Polymer layers bearing poly(ethylene oxide) and phosphorylcholine side chains as non-fouling surfaces: in vitro interactions with plasma proteins and platelets. Acta Biomater. 2011;7:3692–9.
38. Liu S, Chen L, Tan L, Cao F, Bai L, Wang Y. A high efficiency approach for a titanium surface antifouling modification: PEG-o-quinone linked with titanium via electron transfer process†. J Mater Chem B. 2014;2:6758–66.
39. Kizhakkedathu JN, Janzen J, Le Y, Kainthan RK, Brooks DE. Poly(oligo(ethylene glycol)acrylamide) brushes by Surface initiated polymerization: Effect of Macromonomer Chain length on Brush Growth and protein adsorption from blood plasma. Langmuir. 2009;25:3794–801.
40. Feng W, Zhu S, Ishihara K, Brash JL. Protein resistant surfaces: comparison of acrylate graft polymers bearing oligo-ethylene oxide and phosphorylcholine side chains. Biointerphases. 2006;1:50–60.
41. Ortiz R, Olsen S, Thormann E. Salt-Induced Control of the Grafting Density in Poly(ethylene glycol) brush layers by a grafting-to Approach. Langmuir. 2018;34:4455–64.
42. Giamblanco N, Marletta G, Graillot A, Bia N, Loubat Cd, Berret J-F. Serum protein-resistant behavior of multisite-bound poly(ethylene glycol) chains on Iron Oxide surfaces. Acs Omega. 2017;2:1309–20.
43. Joshi O, Lee HJ, McGuire J, Finneran P, Bird KE. Protein concentration and adsorption time effects on fibrinogen adsorption at heparinized silica interfaces. Colloids Surf B-Biointerfaces. 2006;50:26–35.
44. Chen H, Zhang Z, Chen Y, Brook MA, Sheardown H. Protein repellant silicone surfaces by covalent immobilization of poly(ethylene oxide). Biomaterials. 2005;26:2391–9.
45. Roberts JC, Bhalgat MK, Zera RT. Preliminary biological evaluation of polyamidoamine (PAMAM) StarburstTM dendrimers. J Biomed Mater Res. 1996;30:53–65.
46. Hong S, Na YS, Choi S, Song IT, Kim WY, Lee H. Non-covalent self-assembly and covalent polymerization co-contribute to polydopamine formation. Adv Funct Mater. 2012;22:4711–7.
47. Kolewe KW, Dobosz KM, Rieger KA, Chang CC, Emrick T, Schiffman JD. Antifouling Electrospun Nanofiber Mats Functionalized with Polymer Zwitterions. ACS Appl Mater Interfaces. 2016;8:27585–93.
48. Sundaram HS, Han X, Nowinski AK, Brault ND, Li YT, Ella-Menye JR, Amoaka KA, Cook KE, Marek P, Senecal K, Jiang SY. Achieving one-step surface coating of highly hydrophilic poly(carboxybetaine methacrylate) polymers on hydrophobic and hydrophilic surfaces. Adv Mater Interfaces. 2014;1:8.
49. Yeh SL, Deval P, Tsai WB. Fabrication of transparent PEGylated Antifouling Coatings via one-step pyrogallol deposition. Polymers. 2023;15:12.
50. Han Y, Zhao WW, Zheng YW, Wang HM, Sun YL, Zhang YF, Luo J, Zhang HY. Self-adhesive lubricated coating for enhanced bacterial resistance. Bioactive Mater. 2021;6:2535–45.
51. Du MT, Peng MK, Mai BJ, Hu FY, Zhang XD, Chen YS, Wang CH. A multifunctional hybrid inorganic-organic coating fabricated on magnesium alloy surface with antiplatelet adhesion and antibacterial activities. Surf Coat Technol. 2020;384:9.
52. Liu SZ, Zhang Q, Han Y, Sun YL, Zhang YF, Zhang HY. Bioinspired Surface Functionalization of Titanium Alloy for enhanced lubrication and bacterial resistance. Langmuir. 2019;35:13189–95.
53. Nishida K, Anada T, Tanaka M. Roles of interfacial water states on advanced biomedical material design. Adv Drug Deliv Rev 2022, 186.
54. Ma Y, Qiao XY, Lu Q, Li R, Bai YJ, Li X, Zhang SP, Gong YK. Anchorable phosphorylcholine copolymer synthesis and cell membrane mimetic antifouling coating fabrication for blood compatible applications. J Mater Chem B. 2020;8:4299–309.
55. Movafaghi S, Wang W, Bark DL, Dasi LP, Popat KC, Kota AK. Hemocompatibility of super-repellent surfaces: current and future. Mater Horiz. 2019;6:1596–610.
56. Weber M, Steinle H, Golombek S, Hann L, Schlensak C, Wendel HP, Avci-Adali M. Blood-contacting biomaterials: in Vitro evaluation of the hemocompatibility. Front Bioeng Biotechnol. 2018;6:11.
57. Gao Q, Yu M, Su YJ, Xie MH, Zhao X, Li P, Ma PX. Rationally designed dual functional block copolymers for bottlebrush-like coatings: in vitro and in vivo antimicrobial, antibiofilm, and antifouling properties. Acta Biomater. 2017;51:112–24.
58. Yang Y, Qi PK, Wen F, Li XY, Xia Q, Maitz MF, Yang ZL, Shen R, Tu QF, Huang N. Mussel-inspired one-step adherent Coating Rich in Amine groups for Covalent Immobilization of Heparin: Hemocompatibility, Growth behaviors of vascular cells, and tissue response. ACS Appl Mater Interfaces. 2014;6:14608–20.
59. Wu F, Li J, Zhang K, He Z, Yang P, Zou D, Huang N. A multi-functional Coating based on hyaluronic acid and dopamine conjugate for potential application on Surface Modification of Cardiovascular Implanted devices. ACS Appl Mater Interfaces 2015, 8.

60. Mou XH, Miao W, Zhang WT, Wang WX, Ma Q, Du ZY, Li X, Huang N, Yang ZL. Zwitterionic polymers-armored amyloid-like protein surface combats thrombosis and biofouling. Bioactive Mater. 2024;32:37–51.
61. Yang Y, Gao P, Wang J, Tu Q, Bai L, Xiong K, Qiu H, Zhao X, Maitz MF, Wang H et al. Endothelium-Mimicking Multifunctional Coating Modified Cardiovascular Stents via a Stepwise Metal-Catechol-(Amine) Surface Engineering Strategy. *Research* 2020, 2020.

Publisher's note